Available online at www.sciencedirect.com
ScienceDirect
Journal of Asian Earth Sciences 30 (2007) 113–130
Journal of Asian Earth Sciences
www.elsevier.com/locate/jaes

Temperature and age constraints on the metamorphism of the Tethyan Himalaya in Central Nepal: A multidisciplinary approach

C. Crouzet [a], I. Dunkl [b,c,*], L. Paudel [d], P. Árkai [c], T.M. Rainer [e], K. Balogh [f], E. Appel [a]

[a] Institut für Geowissenschaften, Universität Tübingen, Sigwartstrasse 10, D-72076 Tübingen, Germany
[b] Sedimentology and Environmental Geology/GZG, University of Göttingen Goldschmidtstrasse 3, D-37077 Göttingen, Germany
[c] Institute for Geochemical Research, Budaörsi út 45, H-1112 Budapest, Hungary
[d] Central Department of Geology, Tribhuvan University, Kirtipur, Kathmandu, Nepal
[e] Montanuniversität Leoben, Institut für Geowissenschaften Peter Tunner Strasse 5, A-8700 Leoben, Austria
[f] Institute of Nuclear Research, Hungarian Academy of Science, Bem tér 18/c, H-4026 Debrecen, Hungary

Received 4 January 2006; received in revised form 10 July 2006; accepted 17 July 2006

Abstract

Metasediments of Devonian to Triassic age of the Tethyan Himalaya (TH) from several areas in central and western Nepal, between western Dolpo and Marsyandi Valley, were sampled for thermo-metamorphic studies (illite and chlorite ''crystallinity'', vitrinite reflectance, calcite–dolomite and chlorite-chloritoid geothermometers, K/Ar dating on illite-rich fractions and zircon fission track thermochronology). This paper reports, for the first time, the occurrence of chloritoid in the TH out of the range of granite contact aureoles. It also presents the first zircon fission track dating performed on TH metasediments. The peak temperatures of metamorphism have been around 250–300 °C, 320–350 °C, 330–370 °C and 400–450 °C in the western Dolpo, Hidden Valley, Manang and Marpha areas, respectively. In the Manang and Hidden Valley areas, illite K/Ar data are interpreted as ages of recrystallized K-white micas newly formed during metamorphism at around 25–30 Ma. In the Marpha area, illite K/Ar and zircon fission-track ages (12–15 Ma) are consistent representing cooling ages after metamorphic overprinting of higher grade than in the other areas. The joint investigation of the organic maturation and zircon FT chronology yields insight on the thermal calibration of zircon reset. The R_{max} of 5.7% to ~8.0% indicates a temperature range of ca. 315–325 °C which is in the partial annealing zone of the zircon FT thermochronometer. Our results might be explained by the presence of a thick thrust sheet once existing above the study area.

Keywords: Tethyan Himalaya; Geochronology; Geothermometry; Illite ''crystallinity''; Kübler index; Chlorite ''crystallinity''; Vitrinite reflectance; K/Ar; Fission track

1. Introduction

The interest in the thermal history of sedimentary rocks has rapidly grown since the sixties especially in order to predict the timing of oil generation (for review see e.g. Mac Culloh and Naeser, 1989). The transition between diagenesis and low-grade metamorphism can be approached using several methods such as illite Kübler index (''crystallinity'', KI), vitrinite reflectance (VR), conodont colour alteration, fluid inclusions, fission track (FT) thermochronology and clay mineral and zeolite assemblages.

In the Tethyan Himalaya (TH) of central Nepal, most of the previous thermo-metamorphic studies have focused on (1) the granitic bodies and their contact aureole in order to understand their genetics and emplacement mechanisms (see for example Guillot et al., 1995, 1999) and on (2) the relationships between the High Himalayan Crystalline (HHC) and the lower part of the TH (i.e., Godin et al., 1999a; Searle and Godin, 2003). Apart from the studies of Schneider and Masch (1993), Garzanti et al. (1994) and Bollinger et al. (2004), the pressure–temperature–time

* Corresponding author. Tel.: +49 551 39 79 21; fax: +49 551 39 79 96.
E-mail address: istvan.dunkl@geo.uni-goettingen.de (I. Dunkl).

1367-9120/$ - see front matter © 2006 Elsevier Ltd. All rights reserved.
doi:10.1016/j.jseaes.2006.07.014

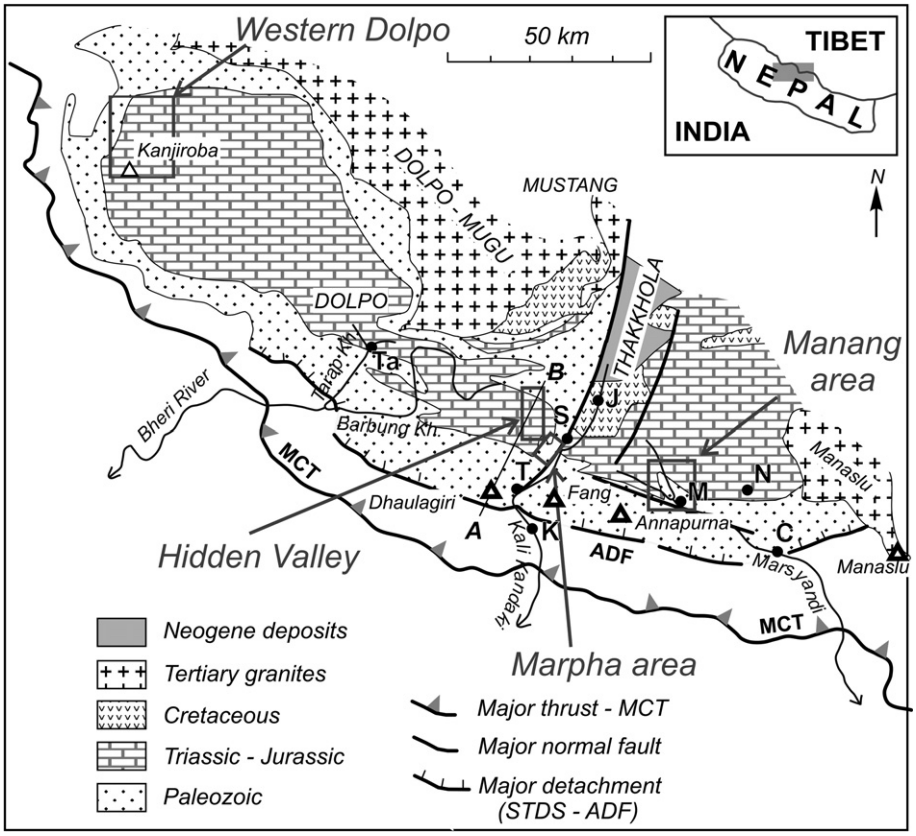

Fig. 1. Simplified geological map of the central Himalaya showing sampling areas (map after Garzanti et al., 1994). MCT: Main Central Trust, STDS: South Tibetan Detachment System (including Annapurna Detachment Fault: ADF). (A–B) location of the cross-section in Fig. 2. K, Kalopani; T, Tukuche; S, Syang; J, Jomosom; M, Manang; C, Chame; N, Nar; Ta, Tarap.

regime of the Himalayan orogeny (upper diagenesis to greenschist facies metamorphism) is still poorly constrained mainly due to the absence of indicative mineralogical assemblages.

The present paper includes analyses of KI, VR, carbonates and chlorite-chloritoid geothermometers, FT thermochronology and K/Ar dating on different grain size of illite–muscovite fractions. Samples from western Dolpo, Hidden Valley, Marpha (western margin of the Thakkhola Graben) and Manang area were studied (Fig. 1). Our multidisciplinary approach improves the knowledge on the metamorphic conditions in different parts of the TH of Nepal and contributes to a better understanding of the validity of the different methods used in low-grade metamorphism.

2. Geological setting

Across its 250–320 km width between the Indus-Tsangpo suture and the Gangetic plain, the 2500 km long Himalayan range is traditionally separated into five major tectono-metamorphic units. These are, from north to south, the Indus-Yarlung suture zone (IYSZ) representing the boundary between the Eurasian and Indian plates, the Tethyan Himalaya (TH), the High Himalayan Crystalline (HHC) thrusting over the Lesser Himalaya, and the Siwaliks (Gansser, 1964; Le Fort, 1975, 1996; Yin and Harrison, 2000; DiPietro and Pogue, 2004). The TH is considered as the stratigraphic cover of the HHC comprising a continuous sedimentary sequence ranging from Cambro-Ordovician to Early Cretaceous in central and western Nepal (Bodenhausen et al., 1964; Bordet et al., 1971; Fuchs, 1977; Bassoulet and Mouterde, 1977; Garzanti and Pagni Frette, 1991; Garzanti, 1999). It is generally interpreted as shelf sediments deposited on the passive northern margin of the Indian Plate (Bassoullet et al., 1980; Brookfield, 1993). An important feature in TH is the North Himalayan antiform, which is widely intruded by granitic bodies. Its southern wedge is underlined by the Kangmar thrust while it is bound to the north by the IYSZ (Burg et al., 1984; Zhang et al., 2004). To the south, the TH is often separated from the metamorphic basement of the HHC by north dipping normal faults which constitute the South Tibetan Detachment System (STDS), first suggested by Caby et al. (1983) and now largely accepted since the work of Burchfield et al. (1992). The high-grade metamorphism of the HHC decreases sharply and quite rapidly from south to north in the TH. In the Kali Gandaki area, the metamorphism reaches lower greenschist facies between Marpha and Syang villages (Garzanti and Pagni Frette, 1991). Southward, the Annapurna detachment juxtaposes psammites of greenschist facies (biotite-muscovite

in the penetrative cleavage) of the Annapurna Yellow Formation of the TH in its hanging wall, with amphibolite facies (biotite-garnet-sillimanite schists) in the footwall (Vannay and Hodges, 1996; Godin et al., 1998; Godin, 2003). This metamorphic gap (transition from sillimanite to greenschist facies) occurs sharply within a few hundred meters (Garzanti and Pagni Frette, 1991). The transition between the amphibolite and greenschist facies rocks is usually considered as the boundary between the HHC and the TH. According to Hodges et al. (1996), this transition is localized in the Cambro-Ordovician metasediments and therefore within in the TH. Searle and Godin (2003) suggest that the lower part of TH has suffered the same metamorphism as its basement and therefore the transition should not be defined as a stratigraphic one but as a metamorphic gap due to tectonic motions.

A major characteristics of the Himalayan belt is the occurrence of granitoid intrusions. In the central part of the mountain belt, three types of plutons occur: (1) the High Himalayan leucogranites, i.e., mainly Everest, Manaslu, Gangotri (Le Fort, 1981, 1986; Le Fort et al., 1987; England et al., 1992; Guillot et al., 1999), (2) the circular bodies of the north Himalayan leucogranite belt (Debon et al., 1986; Zhang et al., 2004) including the Mustang granite (Le Fort and France Lanord, 1995) and (3) the unique huge elongated Mugu-Dolpo pluton (Le Fort and France Lanord, 1995). The TH sediments are locally intruded by Miocene leucogranites. In the studied area, those intrusions are mainly the Mugu-Dolpo granite and the Manaslu granite (Fig. 1). The Manaslu granite is a lenticular body of ~10 km maximum thickness that gently dips to the NNE with a relatively thin sheet, the Chhokang Arm, extending ~60 km to the east of the main body (Harrison et al., 1999). Because the Manaslu intrusive complex crosscuts extensional structures in the hanging wall of the detachment, these features must be older than 19–23 Ma. This is consistent with the ductile motion on the Annapurna detachment which terminated ca. 22 Ma ago (Godin et al., 2001). It should be noticed that Searle and Godin (2003) have a different opinion about the timing of the events.

In the central Himalaya, a major morphological unit is the Thakkhola graben (Fig. 1), a late orogenic extensional structure running north–south between Annapurna and Dhaulagiri ranges. In this structural depression, Cretaceous and Cenozoic sediments are preserved. Outside of the Thakkhola graben, the stratigraphic column ranges from Cambro-Ordovician to middle Jurassic (Fuchs, 1967; Colchen et al., 1986; Fuchs et al., 1988; Colchen, 1999). A major metamorphic gap occurs across the Dangardzong Fault, demarcating the western margin of the Thakkhola graben (Hagen, 1959). The temperature jump is higher than 100 °C corresponding to a vertical offset of more than 3 km (Garzanti and Pagni Frette, 1991).

Polyphase kilometer-scale folds dominate the structural architecture of the TH. The tectonic evolution is usually described by 5 successive deformational phases (Brown and Nazarchuk, 1993; Godin et al., 1999a,b; Godin,

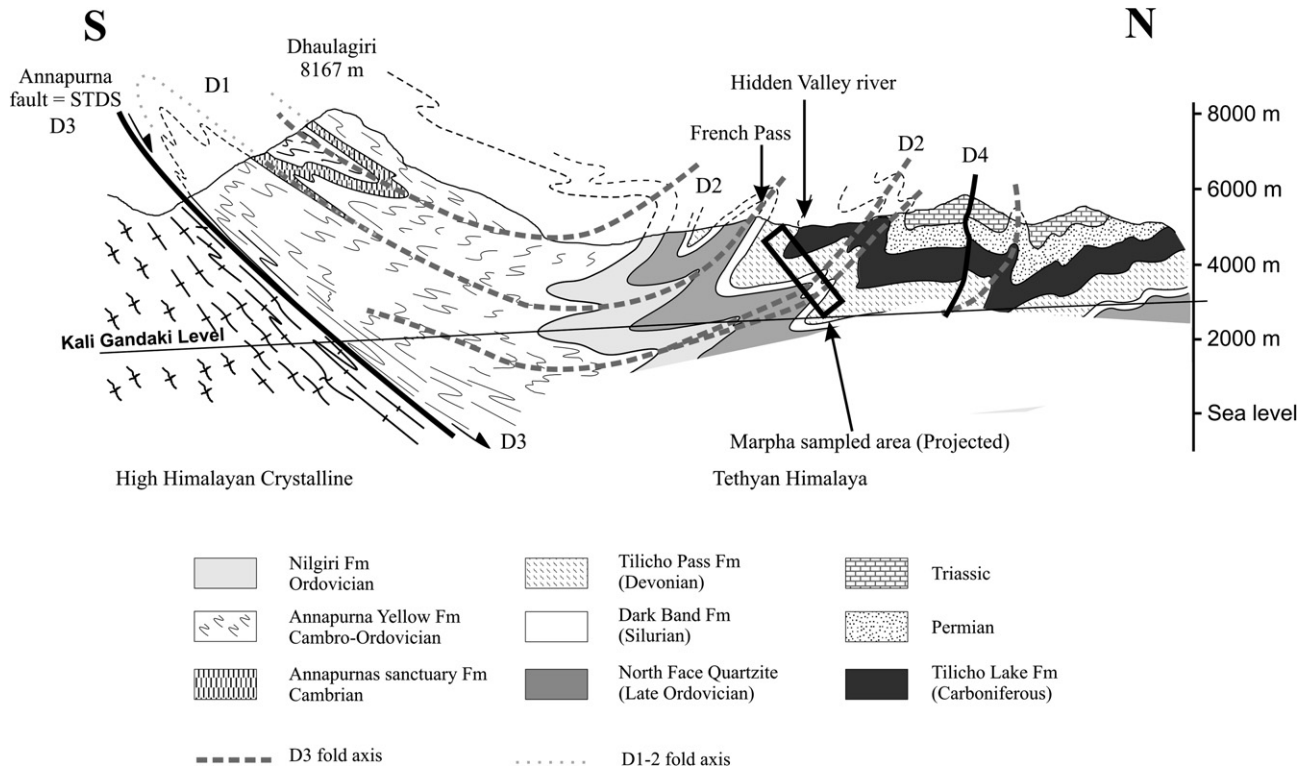

Fig. 2. Geological cross-sections through the Dhaulagiri and Hidden Valley area, according to maps from Fuchs (1967) and Colchen et al. (1986) and our new observations.

2003). The oldest structures (D1) are represented by a cleavage (S1) usually parallel to the bedding (S0) and underlined in the southern part of the TH by biotite and muscovite. F1 folds are visible near the summit of Fang peak where the TH is refolded by D2. F1 folds are usually regarded to be SW vergent. The D2 phase represents the most noticeable structures in the study area (Fig. 2) with many north-vergent folds (F2) known since long. According to Godin et al. (1999a,b), S2 is transposed into a penetrative foliation S3, near the base of the TH. D3 is top to the north as indicated by an SC fabric and micro-folds analysis and is associated with motion along the STDS (Godin et al., 1999a,b; Godin, 2003). D4 structures are characterised by post-metamorphic crenulation cleavage associated with top to the south kink folds. The last deformational event (D5) corresponds to NE–SW trending normal faults associated with the opening of the Thakkhola Graben (Godin et al., 1999a,b; Godin, 2003). In the central Himalaya thrusts affecting the TH are rare. Godin (2003) reports possible thrusting along the Lupra fault north of Jomosom whereas Le Fort and Guillot (1998, 1999) describe an important thrust north of Nar village in the Himlung Himal area. The latter one carries Upper Liassic/Dogger carbonates from the Ratna nappe above Triassic sediments. No other geological surveys have ever revealed thrusts in northern Nepal although they are common far to the W in Zanskar (i.e., Steck et al., 1993; Epard and Steck, 2004).

The Cambrian to Jurassic TH sediments were subjected to a very low to medium grade metamorphism during the Himalayan orogeny (Garzanti et al., 1994). Only few thermometric and geochronological studies have been completed in the TH (Bonhomme and Garzanti, 1991; Wiesmayr and Grasemann, 1999; Wiesmayr, 2000; Williams et al., 2001; Beyssac et al., 2004), and the thermal evolution in the Tethyan sedimentary cover remains still debated.

3. Petrographic characterization of the samples

Location and characteristics of the studied samples are presented in Fig. 3 (see also Appendix A). In the following sections only the most characteristic lithologies are described.

3.1. Carbonates

The Carboniferous and Triassic carbonates are usually siliceous limestones, with micritic and sometimes sparry calcite ranging from 80% to 90% with quartz clasts (10–15%) and about 5% opaque minerals (ilmenite clasts, leucoxene, sulphides and organic matter). Some samples contain a minor amount of detrital mica (<1%). Sparry calcite is more abundant in samples from the lower part of the sedimentary sequence (mainly Tilicho Lake Formation). In the carbonates, fine quartz clasts occur as recrystallized aggregates, while coarse clasts are deformed and elongated along the main foliation. They show undulatory extinction. Some samples contain small veins filled with calcite and/or fibrous quartz. Those veins have been plastically deformed forming ptygmatic and concentric micro-folds.

3.2. Psammitic and pelitic rocks

The Devonian and Permian sandstones and silty, pelitic slate members contain varying amounts of detrital (50–80%) and authigenic (30–50%) minerals. Detrital minerals include quartz, white mica and opaques (mainly ilmenite) and the authigenic minerals include white mica, chlorite, quartz and opaques (graphite, Fe–Ti oxides and sulphides). In sample H0-05 the occurrence of chloritoid indicates a higher metamorphic grade (Vidal et al., 2001; see Fig. 4A). Fine-grained clasts (<0.1 mm) of quartz are deformed to ellipses, arranged parallel to the S1 foliation. Along the quartz tails in the pressure shadows, fine-grained illite–muscovite and chlorite have grown. However, medium- and coarse-grained quartz clasts (>0.1 mm) show very little deformation. They are randomly oriented and the contact between the adjacent grains is straight or slightly curved due to pressure solution. They usually show very weak undulatory extinction. Detrital white micas show random orientations. Recrystallization of white mica, chlorite, and quartz has occurred in the matrix along the major foliation and also in the pressure shadows of the quartz clasts. Recrystallization was found along the S1 and S2 foliations. Opaque minerals usually underline S2 foliation (Fig. 4B).

In all the investigated lithologies, no clear mineralogical transformations were observed. The low-grade metamorphism did not allow index minerals to grow in the studied samples. The newly formed minerals are mainly opaque and small white-micas.

4. Metamorphic and thermochronologic studies

4.1. Illite Kübler index (“crystallinity”) and chlorite “crystallinity”

The illite Kübler index (“crystallinity”, KI) and chlorite “crystallinity” (ChC) results are listed in Table 1. Experimental details are presented in the Appendix B.1. The western Dolpo samples are in the late diagenetic zone (KI = 0.45–0.46Δ°2θ), but all the other samples collected in the surroundings of the Thakkhola graben and in Manang area have suffered anchizonal and epizonal metamorphism. The KI data show that the Tilicho Pass Formation (Devonian) belongs to the epizone, whereas the other overlying sequences belong to the anchizone. The metamorphic grade seems to decrease stratigraphically upward, being consistent with the petrographic observations and literature data. However, no evident trend was found with the present-day elevation or with distance to the HHC. In Hidden Valley, the KI data are around 0.34 Δ°2θ indicating a better crystallization (anchizonal conditions) than in the western Dolpo area. In the Manang and Marpha

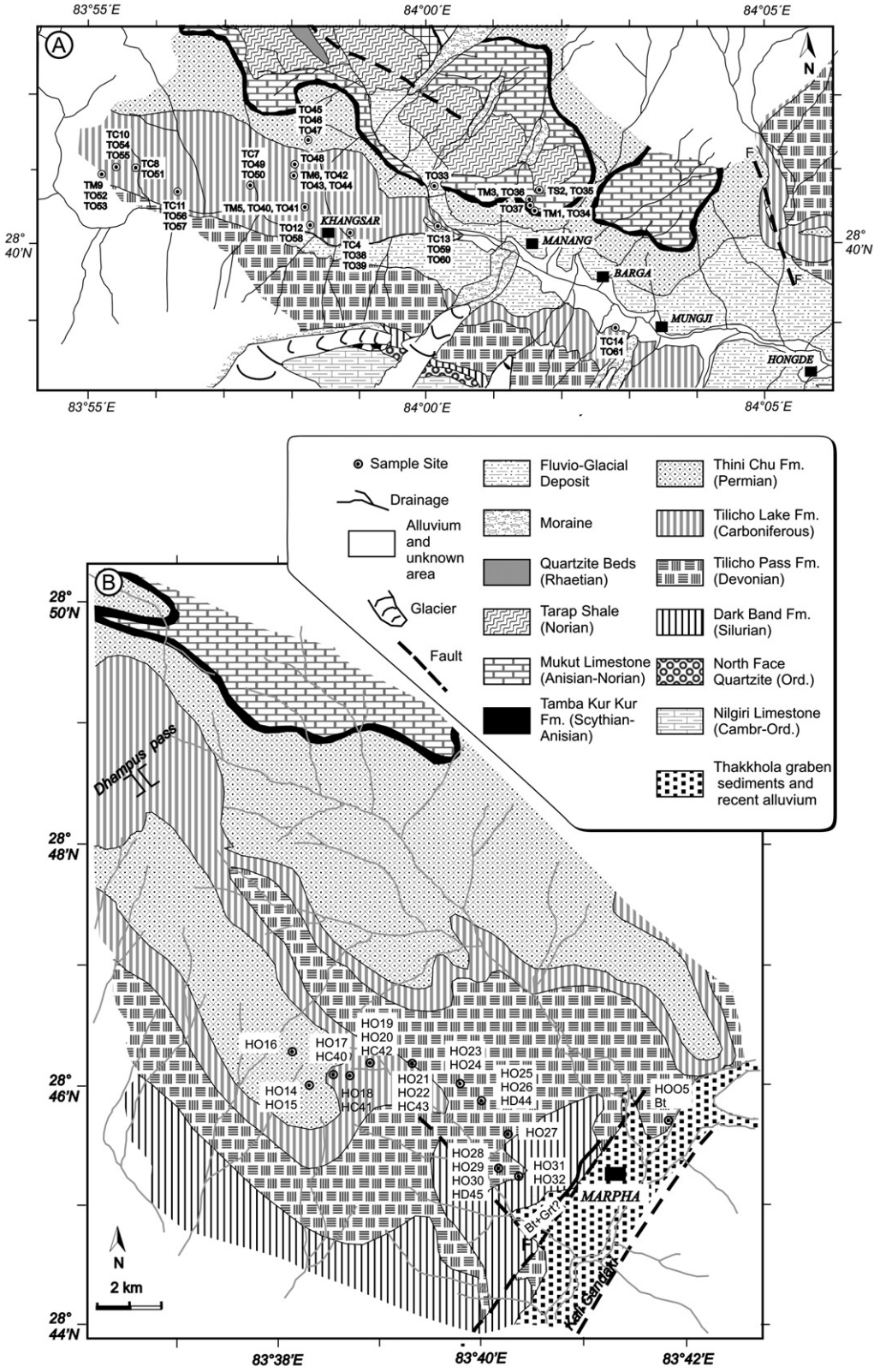

Fig. 3. Geological maps of Manang (A) and Marpha (B) areas with sampling locations. The compilation of these maps is based on the existing geological maps (Fuchs, 1967; Fuchs et al., 1988; Colchen et al., 1986) and our field observations.

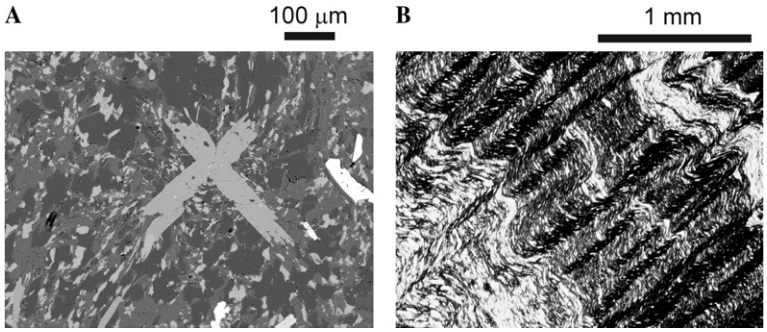

Fig. 4. Representative microphotographs illustrating petrography and micro-scale deformation. (A) Back-scattered electron image of chloritoid (sample H0-05 from Marpha area). (B) Alternating micritic limestone and slate with crenulation clevage (sample TM6-1d from Manang area).

Table 1
Illite and chlorite "crystallinity" data

Sample	KI	ChC(001)	ChC(002)
Marpha area			
HO-5A	0.207	0.208	0.228
H0-14	0.238	0.262	0.274
H0-16	0.280	0.333	0.283
H0-17	0.287	0.284	0.260
H0-18	0.257	0.259	0.244
H0-19	0.285	0.312	0.262
H0-21	0.286	0.311	0.245
H0-25	0.225	0.230	0.234
H0-27	0.229	0.235	0.229
H0-30	0.227	0.223	0.226
H0-32	0.227	0.226	0.233
Manang area			
T0-33	0.298	0.248	0.260
T0-34	0.264	0.257	0.255
T0-35	0.272	0.264	0.253
T0-36	0.403*	0.282	0.275
T0-38	0.216	0.226	0.199
T0-40	0.226	0.223	0.238
T0-43	0.254	0.226	0.243
T0-45	0.485*	0.280	0.267
T0-50	0.281	0.241	0.270
T0-51	0.287	0.303	0.250
T0-52	0.236	0.248	0.226
T0-54	0.275	0.292	0.279
T0-56	0.220	–	0.226
T0-60	0.312*	0.290	0.286
T0-61	0.290	0.331	0.309
Western Dolpo			
I-1	0.450	0.396	0.329
I-2	0.460	0.348	0.327
Hidden Valley			
HM-24	0.336	0.296	0.279

Illite Kübler index (KI) and chlorite "crystallinity" [ChC(001) and ChC(002)] indices measured on <2 μm grain-size air-dried mounts. Values in $\Delta°2\theta$ (Cu Kα). *Samples probably broadened by subordinate paragonite and paragonite/muscovite, therefore inadequate for determining metamorphic grade.

areas, KI results provide mean values of 0.26 ± 0.03 and 0.25 ± 0.03 $\Delta°2\theta$, respectively. Therefore similar metamorphic conditions (lower epizone) may be expected for both areas. In the Devonian and Carboniferous formations, Garzanti et al. (1994) have published KI values from Dangardzong (~0.25 $\Delta°2\theta$) and Syang (~0.45 $\Delta°2\theta$). The new results from Marpha (0.25 ± 0.03 $\Delta°2\theta$) are consistent with those from Dangardzong but are significantly different than those from Syang which are clearly less metamorphosed. KI values from the Manang area (0.26 ± 0.03 $\Delta°2\theta$) are in good agreement with those published by Garzanti et al. (1994). Furthermore, the KI data from Manang and Marpha are also consistent with the crystal-plastic deformation of quartz observed in thin sections. Practically the same conclusions can be drawn from the chlorite "crystallinity" (ChC indices; Table 1). For a detailed explanation of these indices we refer to Árkai et al. (1995b) and Guggenheim et al. (2002).

4.2. Vitrinite reflectance (VR)

VR measurements were carried out on samples from Marpha, Manang and Dolpo areas. The procedure is given in detail in Appendix B.2. Our results indicate clearly that the different areas show different thermal overprint (Table 2 and Fig. 5). The maximum vitrinite reflectance (R_{max}) values of the Marpha, Manang and Dolpo areas are 8.6–10.0%R_{max}, 5.6% and 8.0%R_{max} and 4.8–5.2%R_{max}, respectively. In the different areas, no trends between VR and altitude, distance to HHC or even with stratigraphic position were found. The coal rank of the phytoclasts in the shales of the Manang area reaches the meta-anthracite stage ($R_{min} > 2\%$) according to the German classification (Stach et al., 1982), and the maturation in the Marpha area shows the semi-graphite stage ($R_{min} < 2\%$). This indicates, that thermal maturity in the Marpha area is higher than in the Manang area, and it has reached only the lowest grade in the Dolpo area (Fig. 5). Only sample T0-61 from the Manang area shows 9.2%R_{max} and has similar maturity value to the Marpha samples.

Several approaches have been developed to convert VR data to peak paleotemperature (e.g. Bostick, 1979; Barker, 1988). Random vitrinite reflectance (%R_r) is most widely used as the input parameter. R_r values from Manang samples range from 4.36 to 5.28 %R_r, with an average value of 4.84 %R_r. The PDI-1D thermal modeling software of IES, Jülich (Wygrala, 1988), adopting the extended version of

Table 2
Vitrinite reflectance results: $R_r/R_{max}/R_{min}$: random/maximum/minimum vitrinite reflectance (%), Std: Standard deviation, *n*: number of measurements

Sample name	R_r	Std	*n*	R_{max}	Std	R_{min}	Std	*n*
Marpha area								
HO 14	7.67	0.37	50	9.28	0.88	1.21	0.11	30
HO 16	6.93	0.42	50	9.43	0.85	1.37	0.18	30
HO 17	6.65	0.6	50	9.94	0.9	1.5	0.22	30
HO 19	6.49	0.52	50	8.59	1	1.37	0.14	30
HO 21	6.92	0.51	50	8.97	0.33	1.3	0.14	30
HO 27	6.36	0.56	7	9.06	0.66	1.29	0.13	30
HO 30	6.21	0.41	30	10.02	0.81	1.54	0.19	30
HO 32				9.74	0.35	1.37	0.13	10
Average	6.75			9.38		1.37		
Manang area								
TO 33	4.92	0.34	50	6.07	0.52	2.43	0.72	30
TO 34	4.36	0.28	50	5.81	0.36	2.47	0.67	30
TO 35	5.28	0.43	50	6.38	0.64	2.6	0.36	30
TO 36	5.14	0.42	50	5.68	0.43	2.62	0.46	30
TO 41				5.59	0.72	1.59	0.43	16
TO 45	5.04	0.28	50	6.92	0.6	2.29	0.4	30
TO 50	4.38	0.37	50	6.23	0.64	2.14	0.53	30
TO 53	5.87	0.22	10	8.02	0.8	1.27	0.22	30
TO 54	4.74	0.41	50	6.94	0.68	2.55	0.69	30
TO 56	4.8	0.32	50	7.31	0.68	2.47	0.51	30
TO 60	3.89	0.18	11	6.72	0.85	1.37	0.23	30
TO 61				9.15	1.08	1.2	0.17	30
Average	4.84			6.74		2.08		
Dolpo area								
I1				5.21	0.40	3.07	0.38	11
I2				5.19	0.23	3.00	0.41	30
I3				4.78	0.26	3.08	0.37	30
I4				5.09	0.26	2.70	0.29	30
Average				5.07		2.96		

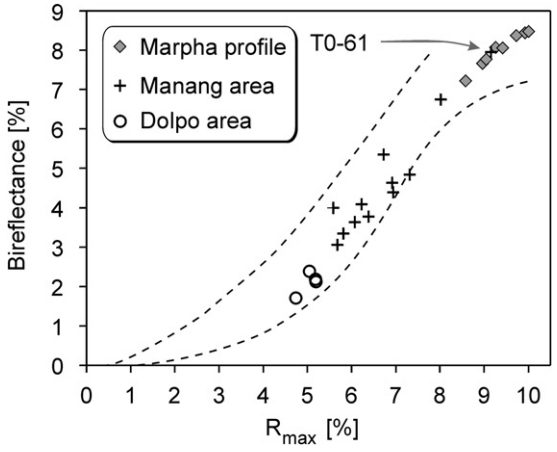

Fig. 5. Vitrinite reflectance data of samples from three study areas. Dashed lines show the empirical envelope of the maturation trend observed in the Mesozoic formation of eastern Swiss Alps (from Ferreiro Mählmann, 1996). The Dolpo, Manang and Marpha samples clearly show different thermal overprint. The exception is sample T0-61 from the Manang area, which suffered similar thermal conditions like the Marpha profile. Only this sample was suitable for calcite–dolomite thermometry (see Fig. 6).

the Easy $\%R_0$ kinetics (Sweeney and Burnham, 1990; Everlien, 1996), was used to estimate the peak paleotemperature. We modelled a pseudo-well, where the Manang samples were close to maximum temperatures for a period of ~5 Myr. In this case, the measured average R_r value corresponds to a temperature of approximately 325 °C. Increasing the assumed time of effective heating to more than 15 Myr results in a temperature of ~315 °C. Using the regression equation of Barker (1988) [$T(°C) = 104$ (ln R_r) + 148] who relates R_r to borehole temperature empirically without considering the effects of heating time, results in a paleotemperature of 312 °C for a VR of 4.84 $\%R_r$.

Problems arise for the peak paleotemperature estimation for the Marpha area because of the extremely high thermal overprint. Most samples show VR > 6.23 $\%R_r$, which is the uppermost limit for the application of the extended version of the Easy $\%R_0$ kinetics (Everlien, 1996). Therefore, neglecting the eventual effect of strain, it can only be presumed that the coalification temperature was above 400 °C.

The role of tectonic stress during the process of coalification is controversial (Ross et al., 1991; Nover et al., 2005). However, Suchy et al. (1997) showed that tectonic deformation may play a major role during the graphitisation. Shear deformation tends to convert vitrinite particles into graphite-like matter. Therefore, tectonic stress (associated with fluid circulation) may have been responsible for the high rank of sample T0-61.

4.3. Calcite–dolomite thermometry

Only one of the investigated samples (T0-61, from Marsyandi valley at Manang) contains coexisting calcite and dolomite crystals (see details in Appendix B.3). Plotting the results in the diagram from Powell et al. (1984), gives a temperature estimate around 360–420 °C (Fig. 6). The X_{Mg}/X_{Fe}(calcite) temperature estimates (see compilation of three calibrations in Dachs, 1990) yield a similar temperature range. The temperature estimates of data points of T0-61 sample indicate an epizonal temperature regime which is in agreement with the vitrinite reflectance data measured on this sample (see Fig. 5).

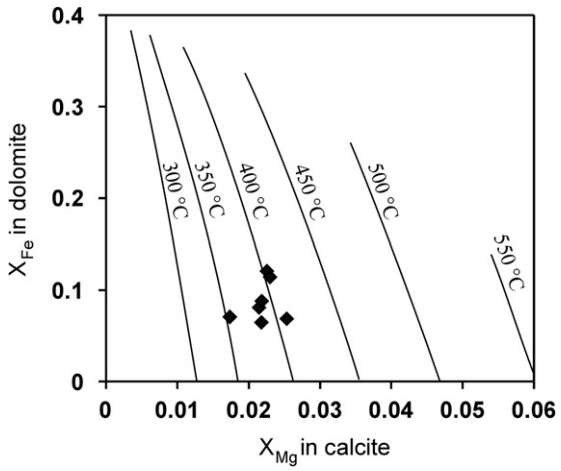

Fig. 6. X_{Mg}(calcite) versus X_{Fe}(dolomite)-diagram (Powell et al., 1984) showing isotherms for coexisting carbonate phases in the sample T0-61.

4.4. Chlorite–chloritoid thermometry

Chloritoid was described in the TH for the first time by Guillot et al. (1995) found in the metamorphic contact aureole of the Manaslu granite. We report here the first occurrence of chloritoids in the TH away from granites (Fig. 4A). The chloritoid stability field depends on the rock chemistry and the Mg and Fe proportion, but usually its presence indicates a temperature of 320–520 °C (Spear, 1993). Chlorite-chloritoid thermometry (using the method of Vidal and Parra (2000) and Vidal et al. (2001)) yields temperature estimation between 420 and 475 °C for the Marpha sample (see analytical details in Appendix B.4).

4.5. K/Ar dating

We have dated the very fine (micron-sized) and presumably newly formed illite fractions from the pelitic rocks using a similar approach than Árkai et al. (1995a) and Dunlap (1997). To minimize the influence of the inherited age of detrital white mica flakes, we have measured K/Ar ages on the finest fractions available from the samples (see details in Appendix B.5). Three size fractions were produced whenever the limited size of the samples allowed it. The difference of ages from the three size fractions reflects the proportion of the newly formed illite although we could not exclude the influence of the detrital grains completely. If the difference of ages is negligible, the age can be considered as a good approximation of the tectono-thermal event responsible for growing of metamorphic new white mica. If the coarser fraction shows a significantly older age, both ages can be interpreted as mixed ages (between the resetting thermal event or mineral formation and the age of the inherited component). In such a case the K/Ar age of the finer fraction is closer to the age of new mica formation, but is not necessarily equal to it (Dunlap, 1997).

4.5.1. Western dolpo

The illite K/Ar chronology (Table 3) from the western Dolpo area yields Late Cretaceous ages (from 71 to 91 Ma). Similar ages were already determined for the High Himalaya (i.e., Sinha, 1989; Metcalfe, 1993) and the TH (i.e., Bonhomme and Garzanti, 1991; Wiesmayr, 2000; Wiesmayr and Grasemann, 1999), using K/Ar method. Illite Kübler indices indicate only a late diagenetic stage, and temperatures were probably neither sufficient for the complete Ar reset nor for dominant illite neo-formation. Therefore, we cannot interpret the results simply as cooling ages. They are rather mixed ages lying between the inherited (pre-sedimentary) age and the Tertiary age of metamorphism (mica neoformation).

4.5.2. Manang and hidden valley areas

In the Manang area the K/Ar ages range from 29 to 41 Ma and from 25 to 31 Ma for the 0.6–2 μm and 0.2–0.6 μm fractions, respectively (Fig. 7). Ages for the Manang samples exhibit wide scatter. Three of the four

Table 3
K/Ar ages for different grain size fractions of the metasedimentary rocks

Sample	Fraction (μm)	K (%)	40Ar(rad) cc STP/g	40Ar(rad) (%)	Age (Ma) ± 1σ
Marpha					
H0-5A	0.6–2	5.258	2.499×10^{-6}	24.0	12.2 ± 0.8
H0-17	0.6–2	5.515	3.274×10^{-6}	41.1	15.2 ± 0.9
H0-18	<0.6	6.547	3.338×10^{-6}	64.6	13.1 ± 0.5
H0-18	0.6–2	6.088	3.478×10^{-6}	67.4	14.6 ± 0.6
H0-19	<0.6	5.103	2.671×10^{-6}	40.1	13.4 ± 0.6
H0-19	0.6–2	4.49	3.416×10^{-6}	49.0	19.5 ± 0.8
H0-25	0.6–2	6.039	3.758×10^{-6}	41.3	15.9 ± 0.8
H0-27	0.6–2	5.956	3.517×10^{-6}	44.5	15.1 ± 0.7
H0-30	0.6–2	5.392	3.083×10^{-6}	45.4	14.6 ± 0.7
Manang					
T0-33	<0.6	6.134	7.001×10^{-6}	55.7	29.1 ± 1.2
T0-33	0.6–2	5.93	6.740×10^{-6}	78.0	29 ± 1.2
T0-33	6–10	3.692	5.326×10^{-6}	88.6	36.4 ± 1.4
T0-35	<0.6	6.492	7.736×10^{-6}	78.2	30.4 ± 1.2
T0-35	0.6–2	6.342	8.696×10^{-6}	74.0	34.5 ± 1.3
T0-50	<0.6	7.095	8.590×10^{-6}	62.8	30.9 ± 1.3
T0-50	0.6–2	6.814	1.100×10^{-5}	83.8	41.1 ± 1.6
T0-50	6–10	4.544	1.075×10^{-5}	91.5	59.9 ± 2.3
T0-51	<0.6	6.859	6.870×10^{-6}	55.4	25.6 ± 1.1
T0-51	0.6–2	6.363	8.623×10^{-6}	65.9	34.5 ± 1.4
T0-54	0.6–2	6.553	1.052×10^{-5}	53.7	40.8 ± 1.7
Dolpo					
I-1	<2	3.651	1.301×10^{-5}	25.9	89.4 ± 5.4
I-2	<2	4.337	1.300×10^{-5}	58.2	75.5 ± 3.1
I-3	<2	5.557	1.553×10^{-5}	90.3	70.5 ± 3.1
I-4	<2	2.783	1.014×10^{-5}	73.5	91.4 ± 2.5
Hidden Valley					
HM-24	<0.6	3.639	4.125×10^{-5}	24.2	29.1 ± 1.8

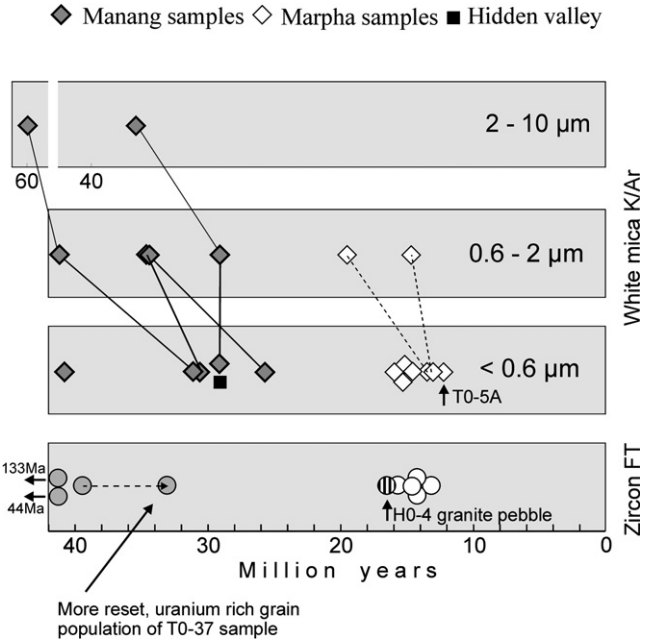

Fig. 7. K/Ar ages measured on different illite fractions (rhombs, lines link the data from different grain size fractions of the same sample) and zircon fission track ages (circles).

grain size couples show significant differences (4–10 Ma or 13–35%). However, in sample T0-33, the two smaller grain size fractions yield identical ages (29 Ma). The KI and VR data for this sample do not explain this behaviour. The K/Ar ages of the finest (<0.6 μm) illite fractions give a cluster between 25 and 32 Ma and the only available sample from Hidden Valley has a similar age (29–30 Ma). According to the zircon FT chronology and thermal estimates (see below), these ages cannot be interpreted as cooling ages. Coleman and Hodges (1998) already reported similar ages (29.9–27.1 Ma) measured on phlogopite and biotite by Ar/Ar method from the TH in Marsyandi Valley samples. Thus, we conclude that the new results from the Manang and Hidden Valley areas represent the age of the formation of new illite-white mica during Eohimalayan metamorphism.

4.5.3. Marpha area

There is a pronounced segregation between the Manang and Marpha samples (Fig. 7 and Table 3). The sampled area of Marpha is situated in the hanging wall of the STDS and west of the main faults limiting the Thakkhola graben. The K/Ar ages are significantly younger than measured in the adjacent areas (12–15 Ma). The results from Marpha show a narrow spread and the difference between the ages of different grain size fractions within a sample is minor (H0-18). This indicates complete neoformation of the micron-sized illite–muscovite. The youngest K/Ar age was obtained on the sample H0-5A which was collected from lowest elevation (at the bottom of the Kali Gandaki Valley). This sample contains chloritoid (Fig. 4A), it has the highest grade of illite crystallinity (Table 1) and the temperature during metamorphism was probably significantly higher than the closure temperature range of K/Ar (see below). Therefore we conclude that the K/Ar ages from Marpha are cooling ages.

4.6. Fission track thermochronology (FT)

The metasedimentary successions of the TH are composed of mainly calcareous and pelitic rocks, the sandy members have a subordinate role and they are usually fine-grained. Nine samples were suitable for fission track chronology, but unfortunately they contain only zircon, but not any apatite. The zircon FT results are listed in Table 4 and the analytical technique is described in the Appendix B.6.

The ages from the Marpha profile are consistent and cluster around 14.4 ± 0.8 Ma. There is no characteristic trend according to the elevation of the samples, but it is noticeable that the sample (H0-5B) collected at the lowest elevation yield the youngest age.

The FT results from the Manang area are older, and they show a scatter from 39 to 133 Ma. This very broad range, and the unexpectedly old, Early Cretaceous age of the T0-47 sample indicate that the zircon FT system underwent only partial resetting during the Oligo-Miocene metamorphism of the TH. The following observations also support this interpretation:

(1) The central ages of the samples have a negative correlation with the uranium content of the dated crystals. The crystal populations with higher U concentration have accumulated a higher density of nuclear damages, thus becoming more sensitive to thermal reset (Blythe, 1996).
(2) The T0-37 sample contains zircon crystal populations of different properties: a rounded, pinkish type and an euhedral, colourless zircon population. It was obvious already during microscopic observation, that the diameter of the tracks strongly varies from grain to grain. Thus, the grains were clustered into two groups: tracks thinner than ~0.5 μm and broader than ~0.8 μm. The thinner tracks were etched mainly in

Table 4
Zircon fission track dating results

Code	Elevation (m)	No.	Spontaneous		Induced		Dosimeter ρd [a]	$P(\chi^2)$ (%)	FT age (Ma ± 1 σ)	Uranium (ppm)
			ρs	(Ns)	ρi	(Ni)				
Marpha profile										
H0-5B	2750	20	25.0	(597)	78.0	(1863)	6.477	13	13.3 ± 0.8	473
H0-15	4940	20	20.7	(628)	59.1	(1789)	6.287	<1	14.3 ± 1.1	362
H0-24	4150	19	21.4	(425)	60.1	(1194)	6.414	31	14.6 ± 0.9	368
H0-26	4000	20	30.2	(455)	86.2	(1297)	6.350	7	14.3 ± 1.0	522
H0-29	3525	20	25.7	(678)	68.3	(1826)	6.446	70	15.5 ± 0.8	408
Manang area										
T0-37	3980	20	44.6	(1950)	45.7	(2001)	6.319	<1	39.3 ± 3.0	319
T0-47	4600	20	117	(2293)	34.6	(674)	6.192	87	133.2 ± 6.4	211
T0-48	4350	20	50.5	(909)	45.2	(813)	6.223	9	44.2 ± 2.7	281

No.: number of dated zircon crystals.
Track densities (ρ) are as measured ($\times 10^5$ tr/cm^2); number of tracks counted (N) shown in brackets.
$P(\chi^2)$: probability obtaining χ^2 value for v degree of freedom (where v = no. crystals-1).
Central ages calculated using dosimeter glass: CN 2 with $\zeta = 127.8 \pm 1.6$.
[a] Nd for all samples: 4543.

the colourless grains and the broader tracks mainly in the pink grains. This phenomenon has an evident correlation with the U content of the grains and its root represents the different densities of radiation damage (α-recoil tracks) of the grains. Splitting the single grain ages of the T0-37 sample into two groups according to the diameter of the tracks these sub-populations have central ages of 33 and 47 Ma – for the broad-track and thin-track populations, respectively.

In the Manang area the zircon FT ages are noticeably older than the K/Ar results of the 0.6–2 μm and 0.6 μm illite fractions although the white mica Ar closure temperature is thought to be higher than closure range of the zircon FT system. This apparent contradiction can be explained by the fact that the micrometer size illite–muscovite crystals are mainly newly formed minerals (with the exception of some minor contribution of detrital mica flakes) and their Ar accumulation started with the crystal growth. The crystal growing temperature can be considerably less than the closure temperature of Ar in illite and also less than the zircon FT system (e.g. Cliff, 1993). Thus, the closure temperature concept cannot be strictly applied to the studied, low-grade rocks.

Joint consideration of the zircon FT and the VR data from the Manang area facilitates the intercalibration of the thermal sensitivity of these systems. The temperature of the annealing of the fission tracks in zircon has been debated for long time (Gleadow et al., 1976). Because the laboratory experiments are rather problematic due to the lack of α-recoil tracks the natural annealing sites controlled by thermometers like organic maturation have a special importance (see review e.g. in Árkai et al., 1995a). The sandstone samples used for FT dating and the slate samples measured by VR were collected not exactly from the same sites, however, the distances are negligible (see Appendix A). The data show that the random VR values from 4.36 to 5.28 $\%R_r$ (~315–325 °C) correspond only to the partial track annealing in zircon. This range is higher than the vitrinite reflectance values $R_r = 2.55$–5.07% reported by Blythe (1996) also from the partial annealing zone of zircon. Very probably the temperature was close to that one needed for a complete reset, but it was still in the partial annealing zone (PAZ). Therefore, the upper limit of the partial annealing zone should be higher than ~325 °C. This point is in agreement with the views of Carpena (1992) estimating the zircon FT closure temperature at around 350 °C, and Tagami and Shimada (1996) estimating the PAZ as ~230 °C to ~330 °C for a heating duration of 1 Myr.

5. Discussion

5.1. Metamorphic temperatures

5.1.1. Inferences from literature

Previously published Himalayan paleotemperature estimations have been deduced mainly from KI and carbonate solvus thermometry. Usually paleotemperatures vary according to the stratigraphic position in the sedimentary sequence. In the Tarap valley of Dolpo, paleotemperature data range from 270 to 400 °C (Garzanti et al., 1994). In the Thakkhola graben, paleotemperature estimates are very low: 70 °C in Cretaceous to 290 °C in Carboniferous strata. For the Manang area and the Marsyandi valley, paleotemperatures of 250–360 °C in Upper Triassic and Jurassic, 270–370 °C in Permo-Carboniferous and 335–530 °C in Cambrian to Devonian are reported (Garzanti et al., 1994; Schneider and Masch, 1993). The highest metamorphic temperatures occurred at the deepest structural levels together with the highest intensity of deformation in the Cambrian-Ordovician limestones (Colchen et al., 1986; Schneider and Masch, 1993; Garzanti et al., 1994). The intensity of tectonic deformation and metamorphic grade decreases progressively northward from amphibolite facies in the early-Palaeozoic metacarbonates to greenschists facies in the mid-Palaeozoic sediments (Fig. 8).

5.1.2. Inferences from quartz and calcite deformation mechanisms

Most of the rocks in the Marpha area are silts and mudstones from the Dark Band formation (Bordet et al., 1971; Colchen et al., 1986) in which some sandy layers are present. Those rocks show strong pressure solution and rare plastic deformation in quartz. The quartz clasts are accompanied by tails of recrystallized quartz. The quartz clasts show strong undulatory extinction. Most of the quartz clasts in the Tilicho Lake and Tilicho Pass formations are elongated parallel to the main foliation (S2). This shows that deformation mechanism in quartz was transitional between dissolution creep and dislocation glide (Passchier and Trouw, 1996; and references cited therein). The above quartz microstructures indicate a temperature >300 °C during deformation (Kerrish et al., 1977; Passchier and Trouw, 1996; Dunlap et al., 1997).

5.1.3. Inferences from KI, VR, calcite–dolomite and chlorite–chloritoid thermometry

Calculation of exact temperature (and pressure) values of diagenetic and very low-grade metamorphism is hindered by several factors. According to the recent review of Merriman and Peacor (1999), clay mineral assemblages as well as crystallinity of certain phyllosilicates like illite–muscovite and chlorite express only the stage that the given assemblage has reached during its transformation through metastable disequilibrium states. Because thermodynamic equilibria have practically never been reached, thermobarometry of these assemblages cannot be elaborated in a strict sense. Unlike higher grade metamorphic rocks, the differences and trends found in temperature or pressure can only be applied for qualitative estimation of changes in physical parameters of metamorphism. Although several attempts have been made in order to constrain the temperature conditions of very low-grade metamorphism (for reviews see Kisch, 1983; Frey, 1987; Merriman and Frey,

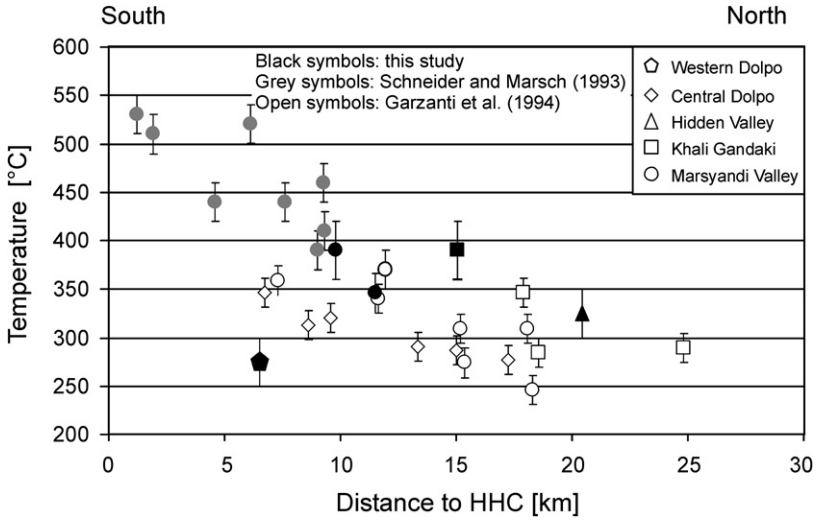

Fig. 8. Shift of metamorphic temperature in TH versus distance to the HHC.

1999). On the basis of these comprehensive works, it is widely accepted that the lower and upper boundaries of the anchizone are at around 200 and 300 °C, respectively.

In spite of these well established theoretical and practical considerations, we have tried to apply various correlations established between the Kübler index and temperature by different authors. Such calibration studies are presented by Underwood et al. (1993) for the Shimanto Accretionary Belt in Japan (with combined study of KI and VR studies), Ji and Browne (2000) for an active geothermal field in New Zealand, and Garzanti et al. (1994) for Himalayan data. Using these calibrations it is possible to estimate, with caution, the temperature reached in our sampling areas from KI values. It must be emphasized, that the quantitative temperatures are only used to express the difference between the various sample groups. In western Dolpo, Hidden Valley and Manang plus Marpha areas, the KI values indicate paleotemperatures around 250–300 °C, 300–350 °C, 320–370 °C, respectively.

Similarly to the KI-based temperature estimates, paleothermometry based on VR is also questionable in the present case. Quantitative models based on the relations between reflectance, temperature and effective heating time were elaborated for lower rank (maturity) organic matters. Thus, the present data sets of VR are at the high-T limit of the T-intervals for which these models can be applied. Vitrinite reflectance data suggest that in the Marpha area, paleotemperatures significantly higher than 400 °C were reached, whereas the Manang data suggest paleotemperatures around 320 °C. The temperature estimation in the Manang area, is consistent with the thermoremanent origin of the magnetization carried by pyrrhotite (Appel et al., 1991; Crouzet et al., 2001b). For the Dolpo area a temperature lower than 280–300 °C can be estimated. In the Manang and Dolpo areas the temperature estimations are consistent with those derived from KI values. Sample T0-61 from the Manang area shows VR values significantly different than the others but very similar to VR values from the Marpha area. Given that T0-61 was used for the calcite/dolomite thermometry this result could be used to estimate the paleotemperatures of the Marpha area. Calcite/dolomite thermometry gives a paleotemperature estimation around 360–420 °C. This is still consistent with estimations from VR values ($T > 400$ °C). The chloritoid/chlorite thermometry performed on a sample (H0-05) from the Marpha area indicates paleotemperatures in the range of 420–475 °C, slightly higher than those estimated from calcite/dolomite thermometry and in good agreement with VR results. The KI value from sample H0-05 gives a temperature estimation of around 335–390 °C. This estimation is significantly different from the result of chlorite/chloritoid thermometry. Sample H0-05 stems from lower altitude than the other samples from the Marpha area. It probably experienced a higher temperature during metamorphism. Considering VR results, calcite/dolomite and chlorite/chloritoid thermometry results, the average temperature in the Marpha area can be estimated at ~400–450 °C. These estimates are significantly different from those derived from KI (320–370 °C) because the illite crystallization becomes ''saturated'' and consequently inaccurate at such elevated temperatures. In addition to temperature, illite ''crystallinity'' is controlled by the strain, mineralogy, whole rock and fluid chemistries (K^+ activity in the pore fluids) and other factors. Therefore, the temperature ranges deduced from KI were not considered in the synthesis. The complete set of new data presented in this paper (Fig. 9) suggests that the average metamorphic temperatures were around 250–300 °C, 320–350 °C, 330–370 °C and 400–450 °C, in the western Dolpo, Hidden Valley, Manang and Marpha areas, respectively.

5.1.4. Consequences

The total thickness of the post-Devonian sedimentary sequence (Carboniferous–Cretaceous) is reported to range

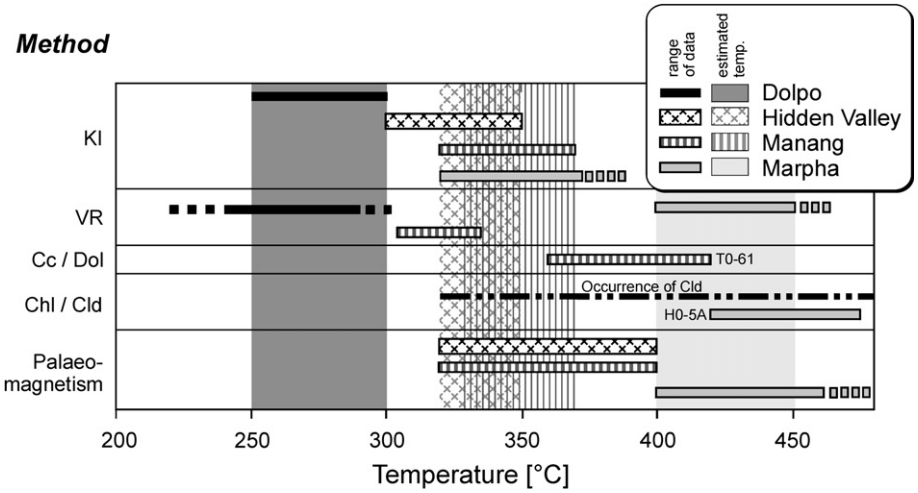

Fig. 9. Synthesis of the metamorphic temperature estimations from the sampled areas using different approaches. The temperature estimation with paleomagnetism are deduced from the thermal origin of the natural remanent magnetization demonstrated by Appel et al. (1991) in Manang and by Crouzet et al. (2001a) in Hidden valley.

from 3900 to 4300 m in the Dolpo-Manang Synclinorium (Colchen et al., 1986; Garzanti, 1999). This sequence was eroded down to Albian level. Based on the succession at Tingri (southern Tibet; Willems et al., 1996), an additional ~1500 m of upper Cretaceous to Eocene marine strata probably overlaid the Albian strata before erosion. The temperatures described above cannot be explained by the thickness of the initial sedimentary sequence (~5500 m) alone unless assuming a very high vertical thermal gradient (~40 °C/km in the western Dolpo and even 80 °C/km in the Marpha area). Such high geothermal gradient should have been associated with granite emplacement or very important fluids circulations. We can reject the hypothesis of high thermal gradient because the presence of hydrothermal veins is negligible and no traces of granite intrusions are known from the investigated areas. Considering a normal geothermal gradient of ~27 °C/km, the temperature should not have exceeded 140–160 °C at the base of the above mentioned ~5.5 km stratigraphic burial. To explain the temperatures observed, we can hypothesize a burial of 9–17 km. While we have no barometric constraints, the burial values estimated above are in very good agreement with the one deduced from the barometric study of Guillot et al. (1995) in the contact aureole of the Manaslu granite. Several explanations can be drawn in order to explain such burial. Based on balanced cross-section and palinspastic restoration in the Kali Gandaki area, Godin (2003) suggests that Ordovician levels were buried up to 20 km after the F2 north verging folding. Therefore the 150% thickening associated to D2 could explain the observed temperature. Whatever, palaeomagnetic investigations performed in the Dolpo-Manang area (Appel et al., 1991; Crouzet et al., 2001a, 2003; Schill et al., 2003) have evidenced a post-deformation remanence acquisition carried by pyrrhotite. This remanence is acquired during the cooling just below 320 °C (Rochette, 1987; Dunlop et al., 2000). It is surprising that those remanence directions are not affected by brittle deformations like the several kink folds described by Godin (2003) as D4. Therefore the thermal climax should be synchronous or postdate D4. A burial of 10 km could be explained by folds and local small thrusts (D4). This can explain paleotemperatures of up to ~270 °C, like in the western Dolpo area. For the other areas, the existence of a major thrust carrying material over the studied areas can be assumed. The existence of such a thrust was proposed by Guillot (1993) and Guillot et al. (1995) in order to justify the barometric results in the contact aureole of the Manaslu granite and more recently by Crouzet et al. (2001a) in order to explain paleotemperatures higher than 325 °C in Triassic metasediments of the Hidden Valley area deduced from palaeomagnetic investigations. Except the Nar Tö thrust, carrying the Ratna nappe over the Triassic of the TH in Himlung Himal area (Le Fort and Guillot, 1998, 1999), no other geological surveys have ever evidenced such a thrust in northern Nepal. The existence of such a thrust, still poorly documented and not well understood, is contested by Fuchs et al. (1999). Also, an hypothetic westward structural prolongation of the Kangmar thrust responsible for the north Himalayan antiform and well evidenced in southern Tibet (Lee et al., 2000, 2004) may be possible north of the studied area. Such thrusts, if existing, may imply a possible late overburden of the studied area.

5.2. Geochronological interpretations

Newly obtained K/Ar data yield Late Paleogene ages in the Hidden Valley (29–30 Ma) and Manang (25–30 Ma) areas. They are interpreted as the age of newly grown fine grained white mica (Fig. 10). Those ages are in good agreement with the ages from Coleman and Hodges (1998) for the lower Marsyandi valley. The zircon FT results show

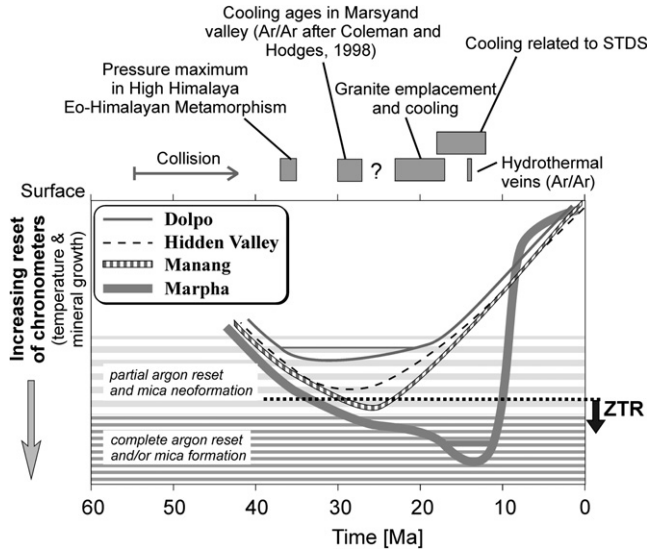

Fig. 10. Summary of reset of the geochronometers. This plot aims to summarise the time of mineral growth and the reset of the different mineral/methods pairs (although they are sensitive to different factors). The Tertiary overprint in Dolpo is practically not datable by the illite K/Ar chronology. In the Hidden Valley and Manang it has reached the maximum intensity during Oligocene, but it was below the temperature of complete reset of zircon FT thermochronometer. On the contrary, in the Marpha profile the climax of the metamorphism took place during Miocene with complete zircon FT and white mica K/Ar reset. ZTR = Zircon Total Reset temperature.

that the Manang area underwent milder thermal overprint, because complete Miocene reset was not observed. The ages between and within the samples show a broad scatter indicating that they were only in the partial annealing zone. The 33 Ma age of the broad-track grain population of the T0-37 sample may be considered as nearly complete reset during Late Paleogene times. This age is remarkably similar to those attributed by Godin et al. (1999b, 2001) to the north verging D2 folds (ca. 35 Ma).

The zircon FT results indicate complete reset of the samples from the Marpha profile during Miocene. For both zircon FT and white mica K/Ar geochronometers, the Marpha area displays the youngest ages (12–15 Ma). The temperature was clearly higher than the zircon FT PAZ. The ages from the Marpha area are in good agreement with those published by Godin et al. (1998, 2001) from the Kali Gandaki region close to and within the HHC and with those from Coleman and Hodges (1995) from an E–W extensional vein. Therefore, the ages reported in the present study may correspond to the initial stage of the extension of the Thakkhola graben and associated processes. Tectonic denudation in the footwall of the normal fault limiting the graben and some local fluid circulations during the opening of the graben may have played an important role within the thermal history of the Marpha area (Fig. 10).

At the scale of the belt, the age of the thermal event in the TH, far from granite emplacement and from STDS, seems to vary from West to East according to K/Ar dating on illite, muscovite and biotite reported in the literature and in the present study. Bonhomme and Garzanti (1991), Wiesmayr (2000), Wiesmayr and Grasemann (1999), Williams et al. (2001) and Coleman and Hodges (1998) report ages around 44–47 Ma in Zanskar, 42–45 Ma in Spiti, ~41.5 Ma in Malari and 26.5–30 Ma in Marsyandi valley. Fig. 11 shows these data in relation to those of the present study. Taken separately, the western part (Zanskar – Malari) and the eastern part (Hidden Valley to Marsyandi) yield ages around 50–40 Ma and 30–25 Ma, respectively. Because no major discontinuity is known to exist between those two areas, we consider this temporal trend to be real. As already suggested by Guillot et al. (1999), a working hypothesis for this migrating tectonothermal evolution could be the initial geometry of the Indian plate and the eastward propagating suturing associated with the counter-clockwise rotation of India.

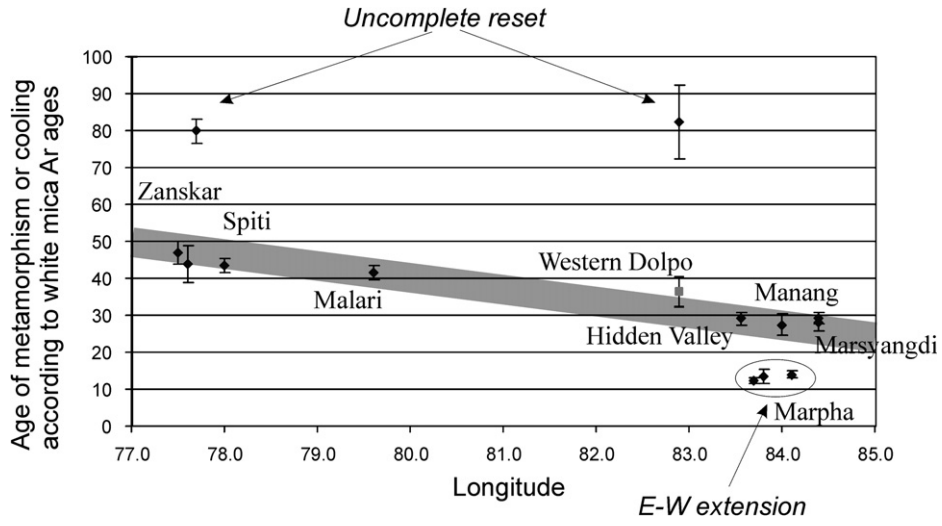

Fig. 11. K(Ar)/Ar ages from the TH (away from STDS and granite outcrops), versus longitude showing a decreasing trend toward east. Sources of data are cited in the text.

6. Conclusions

Although the stratigraphy of the TH is very homogeneous along the entire Himalayan belt, its metamorphic evolution is variable. The multidisciplinary approach presented in this paper is used to characterize the low-temperature metamorphism of the TH from the Dolpo area in the West to the Manang area in the East. The joint investigation of different methods used in this paper, gives important constraints on the interpretations. It is a powerful tool to better control the results from other methods. Previous studies were mainly performed close to granitic bodies or close to the HHC. The present work provides new constraints for the low-grade metamorphic evolution of the TH sedimentary cover itself. Although any single paleotemperature estimate may be uncertain the combination of different methods allow us to quantify the peak paleotemperature in the western Dolpo (Triassic), Hidden Valley (Triassic), Marpha (Devonian–Carboniferous) and Manang (Carboniferous–Triassic) areas at around 250–300 °C, 320–350 °C, 400–450 °C and 330–370 °C, respectively. While no pressure estimation are available, the relatively high temperatures are inferred to result from an important burial explained by: (1) 150% thickening associated to D2 or (2) intra TH important thrust(s) if peak temperature postdate D4 as suggested by palaeomagnetic results.

The age of the metamorphism has been estimated using K/Ar on different size fractions of the metasediments and zircon FT. A cooling age of 12–15 Ma is indicated for the Marpha area. In the Manang area, the peak metamorphic conditions are inferred between 30 and 25 Ma according to K/Ar data.

At the scale of the belt, peak temperatures are diachronous in the TH with ages older in the West and younger toward East. An exception is given by the ages associated to east–west extensional structures such as the Thakkhola graben (i.e., ages ~12–15 Ma in the Marpha area). Therefore, the geodynamic processes may be not so similar along the ~2500 km strike of the Himalayan belt. The data presented in this contribution yield new constraints on the time-temperature evolution of the TH that may be important for future geodynamic models, mountain building processes and reconstruction of the evolution of the Himalayan belt.

Acknowledgements

We acknowledge the helpful advice and re-calculation of the chlorite–chloritoid thermometry with the latest method to O. Vidal (Joseph Fourier University, Grenoble I). Discussion with G. Fuchs is also appreciated. D. Kost, G. Höckh, D. Müllbayer-Renner (Tübingen) and O. Komoróczy (Budapest) assisted during sample preparation. Thanks for their careful work. L. Godin is especially acknowledged for his numerous comments on a previous version. This research was funded by the German Research Foundation (DFG), project AP 34/13-1. The phyllosilicate studies formed a part of the project of P.Á. supported also by the Hungarian National Research Fund (OTKA), Budapest, programme No. T049454.

Appendix A. Location and main characteristics of the studied samples

The table of geographic coordinates of samples giving useful results can be found in a web data repository under the url: http://www.sediment.uni-goettingen.de/staff/dunkl/archive/hidden-valley.

Appendix B. Experimental procedures

B.1. Illite and chlorite "crystallinity"

Metapelites samples were broken into small chips with a jaw crusher and then crushed in a mortar mill for 3 min followed by repeated shaking in deionized water. Aqueous suspensions of the <2 μm fractions were pipetted after appropriate settling time in the sedimentation cylinders and highly oriented sedimentation slides of ca. 3 mg cm^{-2} thickness were prepared. A Philips PW-1730 diffractometer was used for X-ray analysis of the samples under the following conditions: Cu Kα radiation; 45 kV/35 mA; graphite monochromator, proportional counter; divergence and detector slits of 1°; goniometer speed 2°/min and 0.5°/min; time constant 2 s; and chart speed 2 cm/min. Illite "crystallinity" was documented by the Kübler index (abbreviated as KI in Table 1), which is the half width of the 10 Å X-ray diffraction peak of illite above the background (Kübler, 1967 and Kübler and Jaboyedoff, 2000). The KI values were calibrated to those of Kübler's laboratory at Neuchâtel with standard rock slab series (No. 32, 34 and 35).

Chlorite "crystallinity" (ChC), similarly to KI, expresses the stage the chlorite mineral has reached during its reaction progress. It is based on the analogies found between the reaction progress smectite-illite–muscovite and smectite–chlorite (Árkai, 1991). Chlorite "crystallinity" expresses the full-width-at-half-maximum values of the first (14-Å), and second (7-Å) basal reflections of chlorite, measured at conditions similar to KI measurements.

B.2. Vitrinite reflectance

In total 27 samples of black slates were cut, mounted in epoxy resin and polished to estimate the light reflectance of fine dispersed organic matter within the sediment. On 20 samples maximum and minimum VR ($\%R_{max}$; $\%R_{min}$) was determined in monochromatic (546 nm) polarized light. Additionally on 17 samples random VR ($\%R_r$) measurements were done to get input parameter for peak paleotemperature estimation. R_r measurement has to be carried out in monochromatic (546 nm) nonpolarized light (Stach et al., 1982). The measurements were performed on a Leica MPV SP microscope.

B.3. Calcite–dolomite thermometry

Six carbonate thin sections were stained by alizarin red alkaline solution, according to the method outlined in Miller (1988), in order to check the presence of co-existing calcite–dolomite. Only 2 sections showed dolomite (TM9 and T0-61). In specimen TM9, dolomite was present only in veins. However, close observation under the microscope showed that the dolomite and calcite were of different generation. Dolomite is strained and corroded while calcite is unstrained and has sharp grain boundaries. They are no co-existing pairs to be used for thermometry. Specimen T0-61 contained almost equal amount of calcite and dolomite in the groundmass, probably of the same generation. Therefore, calcite–dolomite thermometry was performed in this section. Electron microprobe analyses can be found in the web data repository (www.sediment.uni-goettingen.de/staff/dunkl/archive/hidden-valley).

B.4. Chlorite-chloritoid thermometry

Mineralogical investigations were performed on several samples from different areas in order to detect some index minerals. In one sample from Marpha (H0-05), several chloritoids were found. Therefore, the Chlorite-Chloritoid Mg/Fe exchange thermometry after Vidal et al. (1999), Vidal and Parra (2000) and Vidal et al. (2001) was attempted. The table of electron microprobe analyses can be found in the web data repository (www.sediment.uni-goettingen.de/staff/dunkl/archive/hidden-valley).

B.5. K/Ar geochronology

Twenty-three illite fractions from 16 samples have been dated by the K/Ar method. The selection of samples was made according to the mineral assemblages (whole rock XRD) and the sheet silicate mineralogy was also considered. Separation of different fractions (<0.2, 0.2–0.6, and 0.6–2 μm) from the gently pulverised samples were performed in order to approach the age of latest recrystallisation. The details of the analytical technique can be found in Balogh and Dunkl (2005).

B.6. Zircon Fission Tracks (FT) chronology

Sandstone samples were treated by the common heavy liquid and magnetic separation processes, the zircon crystals were embedded in PFA teflon. For etching the eutectic melt of NaOH–KOH was used at a temperature of 210 °C (Gleadow et al., 1976). From several samples couples of mounts were produced to gain enough, properly etched crystals. The etching time varied from 71 to 129 h. Neutron irradiations were made at the nuclear reactor of Oregon State University (USA). The external detector method was used (Gleadow, 1981), after irradiation the induced fission tracks in the mica detectors were revealed by etching in 40% HF for 30 min. Track counts were made with a Zeiss-Axioskop microscope – computer-controlled stage system (Dumitru, 1993), with magnification of 1000. The FT ages were determined by the zeta method (Hurford and Green, 1983) using age standards listed in Hurford (1998). The error was calculated by using the classical procedure, i.e., by Poisson dispersion (Green, 1981). Calculations and plots were made with the TRACKKEY program (Dunkl, 2002).

References

Appel, E., Müller, R., Widder, R.W., 1991. Paleomagnetic results from the Tibetan Sedimentary Series of the Manang area (north central Nepal). Geophysical Journal International 104, 255–266.

Árkai, P., 1991. Chlorite crystallinity: an empirical approach and correlation with illite crystallinity, coal rank and mineral facies as exemplified by Palaeozoic and Mesozoic rocks of northeast Hungary. Journal of Metamorphic Geology 9, 723–734.

Árkai, P., Balogh, K., Dunkl, I., 1995a. Timing of low-temperature metamorphism and cooling of the Paleozoic and Mesozoic formations of the Bükkium, innermost Western Carpathians, Hungary. Geologische Rundschau 84, 334–344.

Árkai, P., Sassi, F.P., Sassi, R., 1995b. Simultaneous measurements of chlorite and illite crystallinity: a more reliable geothermometric tool for monitoring low- to very low-grade metamorphism in metapelites. A case study from Southern Alps (NE. Italy). European Journal of Mineralogy 7, 1115–1128.

Balogh, K., Dunkl, I., 2005. Argon and fission track dating of Alpine metamorphism and basement exhumation in the Sopron Mts. (Eastern Alps, Hungary): Thermochronology or mineral growth? Mineralogy and Petrology 83, 191–218.

Barker, C.E., 1988. Geothermics of petroleum systems: Implications for stabilization of kerogen maturation after a geologically brief heating duration at peak temperature. In: Magoon, L. (Ed.), Petroleum Systems of the United States, US Geol. Surv. Bull. 1870, pp. 26–29.

Bassoulet, J.P., Mouterde, R., 1977. Les formations sédimentaires Mésozoïques du domaine tibétain de l'Himalaya du Népal. Coll. Int. CNRS, Paris, 268, pp. 53–60.

Bassoullet, J.P., Boulin, J., Colchen, M., Marcoux, J., Mascle, G., Montenat, C., 1980. Evolution des domaines téthysiens au pourtour du bouclier indien du Carbonifère au Crétacé. Géologie des chaînes alpines issues de la Téthys, Colloque C5 du 26ème Congrès Géologique Internat., Paris, Mém. BRGM 115, pp. 180–198.

Beyssac, O., Bollinger, L., Avouac, J.P., Goffe, B., 2004. Thermal metamorphism in the Lesser Himalaya of Nepal determined from Raman spectroscopy of carbonaceous material. Earth and Planetary Science Letters 225, 233–241.

Blythe, A., 1996. Preliminary note on Hf and U concentrations and fission-track annealing in zircon. On Track 6, 3–4.

Bodenhausen, J.W.A., De Booy, T., Egeler, C.G., Nijhuis, H.J., 1964. On the geology of central and west Nepal. A preliminary note. Rep. 22nd Int. Geol. Congr., Delhi 11, pp. 101–122.

Bollinger, L., Avouac, J.P., Beyssac, O., Catlos, E.J., Harrison, T.M., Grove, M., Goffé, B., Sapkota, S., 2004. Thermal structure and exhumation history of the Lesser Himalaya in central Nepal. Tectonics 23/5, TC5015.

Bonhomme, M., Garzanti, E., 1991. Age of metamorphism in the Zanskar Tethys Himalaya (India). Géol. Alpine, Mem. H.S. 16, 15–16.

Bordet, P., Colchen, M., Krummenacher, D., Le Fort, P., Mouterde, R., Rémy, J.M., 1971. Recherches géologiques dans l'Himalaya du Népal, région de la Thakkhola, CNRS, Paris, 279 p.

Bostick, N.H., 1979. Microscopic measurement of the level of catagenesis of solid organic matter in sedimentary rocks to aid exploration for petroleum and to determine former burial temperatures – a review. In: Scholle, P.A., Schluger, P.R. (Eds.), Aspects of diagenesis. SEPM Special Publication 26, pp. 17–43.

Brookfield, M.E., 1993. The Himalayan passive margin from Precambrian to Cretaceous time. Sedimentary Geology 84, 1–35.

Brown, R.L., Nazarchuk, J.H., 1993. Annapurna detachment fault in the Greater Himalaya of Central Nepal. In: Treloar, P.J., Searle, M.P. (Eds.), Himalayan Tectonics, vol. 74. Geological Society Special Publication, London, pp. 461–473.

Burchfield, B.C., Chen, Z., Hodges, K.V., Liu, Y., Royden, L.H., Deng, C., Xu, J., 1992. The southern Tibetan Detachment System, Himalayan orogen: Extension contemporaneous with and parallel to shortening in a collisional mountain belt. Geological Society of America Special Paper 269, 1–41.

Burg, J.P., Guirud, M., Chen, G.M., Li, G.C., 1984. Himalayan metamorphism and deformations in North Himalayan Belt (southern China). Earth and Planetary Science Letters 69, 391–400.

Caby, R., Pécher, A., Le Fort, P., 1983. Le chevauchement central himalayen: nouvelles données sur le métamorphisme inverse à la base de la dalle du Tibet. Rev. Géol dyn. et geogr. Phys. 24 (2), 89–100.

Carpena, J., 1992. Fission track dating of zircon: zircons from Mont Blanc granite (French-Italian Alps). Journal of Geology 100, 411–421.

Cliff, R.A., 1993. Isotopic dating of metamorphism and cooling. In: Funiciello, R., Ricci, C.A., Trommsdorf, V. (Eds.), Proceedings of the VI Summer School Earth and Planetary Siences, Siena, pp. 131–140.

Colchen, M., 1999. The Thakkhola-Mustang graben in Nepal and the late Cenozoic extension in the Higher Himalayas. Journal of Asian Earth Sciences 17, 683–702.

Colchen, M., Le Fort, P., Pêcher, A., 1986. Annapurna, Manaslu, Ganesh Himal. Notice de la carte géologique au 1/200 000éme. Recherches géologiques dans l'Himylaya du Népal. CNRS edition, 136 p, Paris.

Coleman, M., Hodges, K., 1995. Evidence for Tibetan plateau uplift before 14 Myr ago from a new minimum age for east–west extension. Nature 374, 49–52.

Coleman, M., Hodges, K., 1998. Contrasting Oligocene and Miocene thermal histories from the hanging wall and footwall of south Tibetan detachment in the central Himalaya from 40Ar/39Ar thermochronology, Marsyandi Valley, Central Nepal. Tectonics 17, 726–740.

Crouzet, C., Stang, H., Appel, E., Schill, E., Gautam, P., 2001a. Detailed analysis of successive pTRMs carried by pyrrhotite in Himalayan metacarbonates: an example from Hidden Valley, Central Nepal. Geophysical Journal International 146, 607–618.

Crouzet, C., Gautam, P., Appel, E., Schill, E., 2001b. Discussion on new paleomagnetic results from Tethyan Himalaya (Western Nepal): tectonic and geodynamic implications. Journal of Asian Earth Sciences 19 (3A), 11.

Crouzet, C., Gautam, P., Schill, E., Appel, E., 2003. Multicomponent magnetization in Western Dolpo (Tethyan Himalaya, Nepal): implications for tectonic motions. Tectonophysics 377, 179–196.

Dachs, E., 1990. Geothermobarometry in metasediments of the southern Grossvenediger area (Tauern Window, Austria). Journal of Metamorphic Geology 8, 217–230.

Debon, F., Le Fort, P., Sheppard, S.M.P., Sonet, J., 1986. The four plutonic belts of the Transhimalaya-Himalaya: a chemical, mineralogical, isotopic and chronological synthesis along a Tibet-Nepal section. Journal of Petrology 27, 219–250.

DiPietro, J.A., Pogue, K.R., 2004. Tectonostratigraphic subdivisions of the Himalaya; a view from the west. Tectonics 23, 1–20, TC 5001.

Dumitru, T.A., 1993. A new computer-automated microscope stage system for fission-track analysis. Nuclear Tracks and Radiation Measurements 21, 575–580.

Dunkl, I., 2002. TRACKKEY: a Windows program for calculation and graphical presentation of fission track data. Computers & Geosciences 28, 3–12.

Dunlap, W.J., 1997. Neocrystallization or Cooling?: $^{40}Ar/^{39}Ar$ ages of white micas from low grade mylonites. Chemical Geology 143, 181–203.

Dunlap, W.J., Hirth, G., Teyssier, C., 1997. Thermomechanical evolution of a ductile duplex. Tectonics 16, 983–1000.

Dunlop, D.J., Özdemir, Ö., Clark, D.A., Schmidt, P.W., 2000. Time-temperature relations for the remagnetization of pyrrhotite (Fe7S8) and their use in estimating paléo-températures. Earth and Planetery Science Letters 176, 107–116.

England, P., Le Fort, P., Molnar, P., Pêcher, A., 1992. Heat sources for tertiary metamorphism and anatexis in the Annapurna-Manaslu Region Central Nepal. Journal of Geophysical Research 97 (B2), 2107–2128.

Epard, J.-L., Steck, A., 2004. The Eastern prolongation of the Zanskar Shear Zone (Western Himalaya). Eclogae Geologicae Helvetiae 97, 193–212.

Everlien, G., 1996. High-temperature programmed pyrolysis of Paleozoic source rocks from Northern Germany and adjacent areas and its thermodynamic constraints. Organic Geochemistry 24, 985–998.

Ferreiro Mählmann, R., 1996. The pattern of diagenesis and metamorphism by vitrinite reflectance and illite "«crystallinity»" in Mittelbünden and in the Oberhalbstein. Part 2: Correlation of coal petrographical and of mineralogical parameters. Schweizerische Mineralogishe Petrographische Mitteilungen 76, 23–46.

Frey, M., 1987. Very low grade metamorphism of clastic sedimentary rocks. In: Frey, M. (Ed.), Low Temperature Metamorphism. Blackie, Glasgow, pp. 9–58.

Fuchs, G., 1967. Zum Bau des Himalaya. Österreichische Akademie der Wissenschaften 113, 1–212.

Fuchs, G., 1977. The geology of Karnali and Dolpo regions, western Nepal. Jahrbuch Geologische Bundesanstalt 120, 165–217.

Fuchs, G., Widder, R.W., Tuladhar, R., 1988. Contributions to the geology of the Annapurna Range (Manang Area, Nepal). Jahrbuch Geologisches Bundesanstalt 131, 593–607.

Fuchs, G., Regmi, K., Schill, E., 1999. Note on the geology of the Nar-Manang region in the Northern Nepal (Himalaya). 14th Himalaya – Karakoram – Tibet Workshop, abstract volume, Terra Nostra 99/2, pp. 46-47.

Gansser, A., 1964. Geology of the Himalayas. Wiley, New York, 289 p..

Garzanti, E., 1999. Stratigraphy and sedimentary history of the Nepal Tethys Himalaya passive margin. Journal of Asian Earth Sciences 17, 805–827.

Garzanti, E., Pagni Frette, M., 1991. Stratigraphic succession of the Thakkhola region (Central Nepal): Comparison with the Northwestern Tethys Himalaya. Rivista Italiana di Paleontologia e Stratigrafia 97, 3–26.

Garzanti, E., Gorza, M., Martellini, L., Nicora, A., 1994. Transition from diagenesis to metamorphism in the Paleozoic to Mesozoic succession of the Dolpo-Manang synclinorium and Thakkola Graben (Nepal Tethys Himalaya). Eclogae Geologicae Helvetiae 87, 613–632.

Gleadow, A.J.W., 1981. Fission-track dating methods: what are the real alternatives? Nuclear Tracks 5, 3–14.

Gleadow, A.J.W., Hurford, A.J., Quaife, R.D., 1976. Fission track dating of zircon: improved etching techniques. Earth and Planetary Research Letters 33, 273–276.

Godin, L., 2003. Structural evolution of the Tethyan sedimentary sequence in the Annapurna area, central Nepal Himalaya. Journal of Asian Earth Sciences 22, 307–328.

Godin, L., Hodges, K., Parrish, R., Brown, R., 1998. Timing of thermal events in the Upper Kali Gandaki valley of central Nepal Himalaya. 13th Himalayan Karakoram Tibet Workshop, Geological Bulletin, University of Peshawar, Special issue 31, pp. 68–70.

Godin, L., Brown, R.L., Hanmer, S., 1999a. High strain zone in hanging wall of the Annapurna Detachment, central Nepal Himalaya. In: Macfarlane, A., Sorkhabi, R., Quade, J. (Eds.), Himalaya and Tibet: Mountain roots to mountain tops, Geological Society of America, Special Paper 328, pp. 199–210.

Godin, L., Brown, R.L., Hanmer, S., Parrish, R., 1999b. Back folds in the core of the Himalayan orogen: an alternative interpretation. Geology 27, 151–154.

Godin, L., Parrish, R.R., Brown, R.L., Hodges, K.V., 2001. Crustal thickening leading to exhumation of the Himalayan Metamorphic core of central Nepal: Insight from U–Pb geochronology and $^{40}Ar/^{39}Ar$ thermochronology. Tectonics 20, 729–747.

Green, P.F., 1981. A new look at statistics in fission track dating. Nuclear Tracks 5, 77–86.

Guggenheim, S., Bain, D.C., Bergaya, F., Brigatti, M.F., Drits, V.A., Eberl, D.D., Formoso, M.L.L., Galán, E., Merriman, R.J., Peacor, D.R., Stanjek, H., Watanabe, T., 2002. Report of the Association Internationale Pour L'Étude Des Argiles (AIPEA) Nomenclature Committee For 2001: Order, Disorder and Crystallinity in Phyllosilicates and the use of the "Crystallinity Index". Clays and Clay Minerals 50, 406–409.

Guillot, S., 1993. Le granite de Manaslu (Népal central). Marqueur de la subduction et de l'extension intracontinentales himalayennes. Etude structurale, métamorphique et géochimique. Géologie Alpine, mémoire H.S. 19, 97p.

Guillot, S., LeFort, P., Pêcher, A., 1995. Contact metamorphism and depth of emplacement of the Manaslu granite (central Nepal). Implications for Himalayan orogenesis. Tectonophysics 241, 99–119.

Guillot, S., Cosca, M., Allemand, P., Le Fort, P., 1999. Contrasting metamorphic and geochronologic evolution along the Himalayan belt. In: Macfarlane, A., Sorkhabi, R., Quade, J. (Eds.), Himalaya and Tibet: Mountain roots to mountain tops, Geological Society of America, Special Paper 328, pp. 117–128.

Hagen, T., 1959. Geologie des Thakkhola (Nepal). Eclogae Geologicae Helveticae 52, 709–720.

Harrison, T., Grove, M., McKeegan, K., Coath, C.D., Lovera, O.M., Le Fort, P., 1999. Origin and episodic emplacement of the Manaslu intrusive complex, Central Himalaya. Journal of Petrology 40, 3–19.

Hodges, K., Parrish, R.R., Searle, M.P., 1996. Tectonic evolution of the central Annapurna Range, Nepalese Himalayas. Tectonics 15, 1264–1291.

Hurford, A.J., 1998. Zeta: the ultimate solution to fission-track analysis calibration or just an interim measure? In: Van den haute, P., De Corte, F. (Eds.), Advances in Fission-track Geochronology. Kluver Academic Publishers, Dordrecht, The Netherlands, pp. 19–32.

Hurford, A.J., Green, P.F., 1983. The zeta age calibration of fission-track dating. Chemical Geology 41, 285–317.

Ji, J., Browne, P.R.L., 2000. Relationship between illite "crystallinity" and temperature in active geothermal systems of New Zealand. Clays and Clay Minerals 48, 139–144.

Kerrish, R., Beckinsale, R.D., Durham, J.J., 1977. The transition between deformation regimes dominated by intercrystalline diffusion and intracrystalline creep evaluated by oxygen isotope thermometry. Tectonophysics 38, 241–257.

Kisch, H.-J., 1983. Mineralogy and petrology of burial diagenesis (burial metamorphism) and incipient metamorphism in clastic rocks. In: Larsen, G., Chilingar, G.V. (Eds.), Diagenesis in Sediments and Sedimentary Rocks. Elsevier, Amsterdam, pp. 289–493.

Kübler, B., 1967. La cristallinité de l'illite et les zones tout à fait supérieures du métamorphisme. In: Etages tectoniques (Colloque de Neuchâtel, 18-21 avril 1966). Neuchâtel, Univ., Inst. Geol. pp. 105–122.

Kübler, B., Jaboyedoff, M., 2000. Illite crystallinity. Compte Rendu de l'Académie des Sciences, Paris, Earth and Planetary Sciences 331, 75–89.

Lee, J., Hacker, B., Dinklage, W.S., Wang, Y., Gans, P., Calvert, A., Wan, J.-P., Chen, W., Blythe, A.E., McClelland, W., 2000. Evolution of the Kangmar Dome, southern Tibet: structural, petrologic and thermochronologic constraints. Tectonics 19, 872–895.

Lee, J., Hacker, B., Yu Wang, 2004. Evolution of North Himalayan Gneiss Domes: structural and metamorphic studies in Mabja Dome, southern Tibet. Journal of Structural Geology 26, 2297–2316.

Le Fort, P., 1975. Himalayas: the collided range. Present knowledge of the continental arc. American Journal of Science A 275, 1–44.

Le Fort, P., 1981. Manaslu leucogranite: a collision signature of the Himalaya. A model for its genesis and emplacement. In: Barker, F. (Ed.), Granites and rhyolites, Journal of Geophysical Research 86, B11, pp. 10545–10568.

Le Fort, P., 1986. The 500 Ma magmatic event in Alpine Southern Asia episode at Gondwana scale. Mémoire Sciences de la Terre, Nancy 47, 191–209.

Le Fort, P., 1996. Evolution of the Himalaya. In: Yin, A., Harrison, T.M. (Eds.), The Tectonic Evolution of Asia. Cambridge University Press, Cambridge, pp. 95–109.

Le Fort, P., France Lanord, C., 1995. Granites from Mustang and surrounding regions (Central Nepal). Journal of Nepal Geological Society 11, 53–58.

Le Fort, P., Guillot, S., 1998, Preliminary results of Himlung expedition to northern Manaslu massif, central Nepal. In: Hamidullah, S., Robert, L.D., Qasim, J.M. (Eds.), 13th Himalaya-Karakoram-Tibet international workshop; abstract volume.; Geological Bulletin, University of Peshawar. 31, pp. 110–112.

Le Fort, P., Guillot, S., 1999, Expédition Himlung Himal 1997, une carte géologique. Les cahiers du Comité Scientifique du Club Alpin Français.

Le Fort, P., Cuney, M., Deniel, C., France-Lanord, C., Sheppard, S.M.F., Upreti, B.N., Vidal, P., 1987. Crustal generation of the Himalayan leucogranites. Tectonophysics 134, 39–57.

Mac Culloh, T.H., Naeser, N.D., 1989. Thermal history of sedimentary basins; introduction and overview. In: Naeser, N.D., McCulloh, T.H. (Eds.), Thermal History of Sedimentary Basins; Methods and Case Histories. Springer Verlag, New York, pp. 1–11.

Merriman, R.J., Frey, M., 1999. Patterns of very low-grade metamorphism in metapelitic rocks. In: Frey, M., Robinson, D. (Eds.), Low-Grade Metamorphism. Blackwell Science, Oxford, pp. 61–107.

Merriman, R.J., Peacor, D.R., 1999. Very low-grade metapelites: mineralogy, microfabrics and measuring reaction progress. In: Frey, M., Robinson, D. (Eds.), Low-Grade Metamorphism. Blackwell Science, Oxford, pp. 10–60.

Metcalfe, R.P., 1993. Pressure, temperature and time constraints on the metamorphism across the Main Central Thrust zone and High Himalayan Slab in the Garhwal Himalaya. In: Treloar, P.J., Searle, M.P. (Eds.), Himalayan Tectonics, Geological Society Special Publication, pp. 485–509.

Miller, J., 1988. Microscopical techniques; I, Slices, slides, stains and peels. In: Tucker, M. (Ed.), Techniques in Sedimentology. Blackwell Science, Oxford, pp. 86–107.

Nover, G., Stoll, J.B., von der Gönna, J., 2005. Promotion of graphite formation by tectonic stress – a laboratory experiment. Geophysical Journal International 160, 1059–1067.

Passchier, C.W., Trouw, R.A.J., 1996. Microtectonics. Springer Verlag, Berlin, 289 p..

Powell, R., Condliffe, D.M., Condliffe, E., 1984. Calcite–dolomite geothermometry in the system $CaCO_3$–$MgCO_3$–$FeCO_3$: an experimental study. Journal of Metamorphic Geology 2, 33–41.

Rochette, P., 1987. Metamorphic control of the magnetic mineralogy of black shales in the Swiss Alps, toward the use of "magnetic isograde". Earth and Planetary Science Letters 84, 446–456.

Ross, J.V., Bustin, R.M., Rouzaud, J.N., 1991. Graphitization of high rank coals, the role of shear strain; experimental considerations. Organic Geochemistry 17, 585–596.

Schill, E., Appel, E., Godin, L., Crouzet, C., Gautam, P., Regmi, K., 2003. The influence of deformation on secondary magnetic inclinations in the Nar/Phu valley (central Nepal). Tectonophysics 377, 197–209.

Schneider, C., Masch, L., 1993. The metamorphism of the Tibetan Series from the Manang area Marsyangdi Valley, Central Nepal. In: Treloar, P.J., Searle, M.P. (Eds.), Himalayan Tectonics, Geological Society, Special Publication, London, 74, pp. 357–374.

Searle, M.P., Godin, L., 2003. The south Tibetan detachment and the Manaslu leucogranite: a structural reinterpretation and restoration of the Annapurna–Manaslu Himalaya, Nepal. Journal of Geology 111, 505–523.

Sinha, A.K., 1989. Geology of the higher Central Himalaya. Wiley, Chichester, UK, 219 p..

Spear, F.S., 1993. Metamorphic Phase Equilibria and Pressure–Temperature–Time Paths. Mineralogical Society of America, Washington, USA, 799 p..

Stach, E., Teichmüller, M.Th., Teichmüller, M., Taylor, G.H., Chandra, D., Teichmüller, R., 1982. Stach's Textbook of Coal Petrology. third ed. Borntraeger, Berlin, pp. 1–535..

Steck, A., Spring, L., Vannay, J.-C., Masson, H., Bucher, H., Stutz, E., Marchant, R., Tièche, J.-C., 1993. Geological transect across the North-western Himalaya Eastern Ladakh and Lahul (A model for the continental collision of India and Asia). Eclogae Geologicae Helvetiae 86, 219–263.

Suchy, V., Frey, M., Wolf, M., 1997. Vitrinite reflectance and shear-induced graphitisation in orogenic belts: A case study from the Kandersteg area, Helvetic Alps, Switzerland. International Journal of Coal Geology 34, 1–20.

Sweeney, J.J., Burnham, A.K., 1990. Evaluation of a simple model of vitrinite reflectance based on chemical kinetics. American Association Petroleum Geologists Bulletin 74, 1559–1570.

Tagami, T., Shimada, C., 1996. Natural long-term annealing of the zircon fission track system around a granitic pluton. Journal of Geophysical Research 101 (B4), 8245–8255.

Underwood, M.B., Laughland, M.M., Kang, S.M., 1993. A comparison among organic and inorganic indicators of diagenesis and low-temperature metamorphism, Tertiary Shimanto Belt, Shikoku, Japan. Geological Society of America Special Paper 273, 45–61.

Vannay, J.C., Hodges, KV., 1996. Tectonometamorphic evolution of the himalayan metamorphic core between the Annapurna and Dhaulagiri, central Nepal. Journal of Metamorphic Geology 14, 635–656.

Vidal, O., Parra, T., 2000. Exhumation paths of high pressure metapelites obtained from local equilibria for chlorite–phengite assemblages. Geological Journal 35, 139–161.

Vidal, O., Goffé, B., Bousquet, R., Parra, T., 1999. Calibration and testing of an empirical chloritoid–chlorite Mg–Fe exchange thermometer and thermodynamic data for daphnite. Journal of Metamorphic Geology 17, 25–39.

Vidal, O., Parra, T., Trotet, F., 2001. A thermodynamic model for Fe–Mg aluminous chlorite using data from phase equilibrium experiments and natural pelitic assemblages in the 100 °C to 600 °C, 1 to 25 kb range. American Journal of Sciences 301, 557–592.

Wiesmayr, G., 2000. Eohimalaya structural evolution of the fold and thrust belt in the Tethyan Himalaya (Spiti, N-India). Ph.D. Thesis, University of Wien, 103pp.

Wiesmayr, G., Grasemann, B., 1999. Balanced cross-section and depth to detachment calculations for the Tethyan Himalaya (Spiti, N India): Where is the crystalline basement of the Higher Himalaya? 14th HKTW. Terra Nostra 2, 172–173.

Willems, H., Zhou, Z., Zhang, B., 1996. Stratigraphy of the upper cretaceous and lower tertiary strata in the Tethyan Himalayas of Tibet (Tingri area, China). Geologische Rundschau 85, 723–754.

Williams, H., Prince, C., Argles, T., Harris, N.B.W., 2001. Thermal evolution of the Himalayan metamorphic belt, Garhwal, India: constraints from ^{40}Ar–^{39}Ar and Sm–Nd data. Journal of Asian Earth Sciences 19 (3A), 75.

Wygrala, B.P., 1988. Integrated computer-aided basin modeling applied to analysis of hydrocarbon generation history in a Northern Italian oil field. Organic Geochemistry 13, 187–197.

Yin, A., Harrison, T.M., 2000. Geologic evolution of the Himalayan-Tibet orogen. Annual Review of Earth and Planetary Sciences 28, 211–280.

Zhang, H., Harris, N., Parrish, R., Kelley, S., Zhang, L., Rogers, N., Argles, T., King, J., 2004. Causes and consequences of protracted melting of the mid-crust exposed in the North Himalayan antiform. Earth and Planetary Science Letters 228, 195–212.